Journal of Power Sources 196 (2011) 10148–10155

Contents lists available at ScienceDirect

Journal of Power Sources

journal homepage: www.elsevier.com/locate/jpowsour

Solution combustion synthesis of layered $LiNi_{0.5}Mn_{0.5}O_2$ and its characterization as cathode material for lithium-ion cells

P. Manikandan, M.V. Ananth*, T. Prem Kumar, M. Raju, P. Periasamy, K. Manimaran

Lithium Battery Group, Electrochemical Power Sources Division, CSIR-Central Electrochemical Research Institute, Karaikudi 630 006, India

ARTICLE INFO

Article history:
Received 20 May 2011
Received in revised form 14 July 2011
Accepted 5 August 2011
Available online 12 August 2011

Keywords:
$LiNi_{0.5}Mn_{0.5}O_2$
Lithium ion battery
Layered structure
Cathode material
Combustion synthesis

ABSTRACT

$LiNi_{0.5}Mn_{0.5}O_2$, a promising cathode material for lithium-ion batteries, is synthesized by a novel solution-combustion procedure using acenaphthene as a fuel. The powder X-ray diffraction (XRD) pattern of the product shows a hexagonal cell with $a = 2.8955$ Å and $c = 14.1484$ Å. Electron microscopy investigations indicate that the particles are of sub-micrometer size. The product delivers an initial discharge capacity of 161 mAh g^{-1} between 2.5 and 4.6 V at a 0.1 C rate and could be subjected to more than 50 cycles. The electrochemical activity is corroborated with cyclic voltammetric (CV) and electrochemical impedance data. The preparative procedure presents advantages such as a low cation mixing, sub-micron particles and phase purity.

1. Introduction

The common cathode material in commercial lithium-ion batteries is $LiCoO_2$. Because of the high cost and toxicity of cobalt [1], the industry, in weaning away from cobalt, is on the lookout for alternatives such as lithium nickel manganese oxides that exhibit higher capacities and improved safety [2]. $LiNi_{0.5}Mn_{0.5}O_2$ is particularly attractive due to its higher specific capacity, lower cost and excellent thermal stability [3]. Moreover, $LiNi_{0.5}Mn_{0.5}O_2$ undergoes only marginal volume changes during charge–discharge processes [4].

The applicability of $LiNi_{0.5}Mn_{0.5}O_2$ as a cathode material, however, is limited by its poor rate capacity due to poor electronic conductivity [5] and cycle instability [6]. In addition, stoichiometric phases are difficult to prepare [7] especially by the conventional solid state fusion method [8]. Hence, there is a need to explore synthetic strategies to obtain phase-pure $LiNi_{0.5}Mn_{0.5}O_2$ with desirable electrochemical properties [9]. Efforts are, therefore, being made to explore new synthesis routes with different starting materials to overcome these drawbacks.

$LiNi_{0.5}Mn_{0.5}O_2$ has a rhombohedral layered structure with space group $R\bar{3}m$, and is built on a consecutive arrangement of lithium and transition metal ions in a close-packed oxygen array, leading to the formation of discrete lithium and transition metal layers [10]. About 8–10 at.% of nickel and lithium ions interchange their sites in the layered structure, which is often referred to cation mixing, and noticed in products obtained at high temperatures [11]. While nickel, which is electrochemically active [12], is present in the +2 state, the manganese in this compound is present in the +4 state. $LiNi_{0.5}Mn_{0.5}O_2$ exhibits some structural peculiarities such as partial mixing of lithium and nickel ions between the layers leading to cation disorder [13] and a tendency of the Li^+ and Mn^{4+} ions towards ordering in the layers [14].

The electrochemical performance of these electrode materials is strongly dependent on the synthesis procedure [15]. Various synthesis methods like solid-state reaction [3,8,11], ion-exchange [16], hydroxide co-precipitation [13,17], hydrothermal synthesis [18], ultrasonic assistance synthesis [19], glycine assisted combustion (GAC) [20], mixed hydroxide [17], ball milling [21], ultrasonic agitation [19], oxalate co-precipitation [22], etc., have been adopted to prepare this material. It is, however, difficult to obtain higher battery-active $LiNi_{0.5}Mn_{0.5}O_2$ either due to substantial Li/Ni disorder [16] or structural impurity [23]. In this paper, the structural and electrochemical properties of $LiNi_{0.5}Mn_{0.5}O_2$ prepared by acenaphthene-assisted solution combustion (AASC) process are studied.

2. Experimental

Stoichiometric amounts of lithium nitrate (3.0241 g) with 5 wt.% excess, nickel nitrate (6.0738 g) and manganese nitrate (5.2425 g) were dissolved in a minimum amount of water. Acenaphthene (1.6658 g) was also dissolved in 30 ml glacial acetic acid. The nitrates and the fuel were mixed, transferred into a 300 ml

* Corresponding author. Tel.: +91 4565227553; fax: +91 4565227713.
E-mail address: mvananth@rediffmail.com (M.V. Ananth).

0378-7753/$ – see front matter © 2011 Elsevier B.V. All rights reserved.
doi:10.1016/j.jpowsour.2011.08.034

alumina crucible, and introduced into a muffle furnace pre-heated to 450 °C. The furnace was maintained at 450 °C for 15 min and then allowed to cool naturally. The product formed was ground well and calcined at 600, 700, 800, 900 and 1000 °C for 12 h. Phase formation was analyzed by X-ray diffraction (Bruker D8 Advance X-ray diffractometer) using Cu K_α radiation. Morphological examinations were made by a Hitachi S-3000H scanning electron microscope (SEM) and a Technai 20 transmission electron microscope (TEM) operated at 200 kV. Electron paramagnetic resonance (EPR) studies were made by a Bruker EMX plus X-band spectrometer. X-ray photoelectron spectroscopic (XPS) studies were conducted using a Thermoscientific, UK Multilab 2000 electron spectroscope with Al K_α radiation and at a scan range of 0–1200 eV binding energy (BE). Cyclic voltammograms were recorded at a scan rate of 0.1 mV s^{-1} between 2.5 and 4.6 V. Electrochemical impedance spectroscopy (EIS) analysis was done over a frequency range of 100 kHz–0.1 Hz. An Autolab electrochemical workstation (PGSTAT30) was employed for the CV and EIS studies. Lithium insertion behavior was evaluated by an Arbin multichannel charge–discharge instrument (BT2000). Coin cells of the CR2032 configuration were assembled using lithium foil (thickness: 0.75 mm) as the anode and $LiNi_{0.5}Mn_{0.5}O_2$ as the cathode. A 1 M solution of $LiPF_6$ in 1:1 (v/v) EC–DMC mixture was used as the electrolyte. The cathode was fabricated by blade-coating slurry of 80 wt.% $LiNi_{0.5}Mn_{0.5}O_2$, 15 wt.% SP-carbon (Timcal) and 5 wt.% PVdF in NMP on to an aluminum foil. The cells were assembled in an argon-filled glove box (mBRAUN MB200G) with oxygen and moisture levels less than 0.1 ppm. Galvanostatic charge–discharge studies were run between 2.5 and 4.6 V at a 0.1 C rate.

3. Results and discussion

Lithium transition metal oxides can be elegantly and rapidly synthesized by solution-combustion process (self propagating high temperature, furnace less or fire synthesis) rather than by conventional, high-temperature, solid-state synthesis [24]. The procedure consists of addition of a mild fuel to the nitrate based precursors and ignition at selected temperature. Combustion is accompanied by simultaneous decomposition of nitrate and oxidation of the metal, resulting in the formation of the metal oxide. An outstanding feature in this process is the evolution of large quantities of gases, which yields large surface area particles of sinter-active submicron sizes. The fuel plays a crucial role in this process. Reports suggest that during the solution combustion synthesis of $LiNi_{0.5}Mn_{0.5}O_2$, relevant chemical reactions occur near 450 °C [9]. The calcination temperature for the prepared layered $LiNi_{0.5}Mn_{0.5}O_2$ should, therefore, be higher than 450 °C, and accordingly calcinations have been carried out in this study.

3.1. Structural characterization of materials

3.1.1. X-ray diffraction studies

The powder XRD patterns of the products obtained by calcination at different temperatures for 12 h are shown in Fig. 1. The broad peaks observed in the case of the material calcined at 600 °C indicate that the material is poorly crystalline. It can be seen from the figure that the crystallinity of material improves with increasing calcination temperature. Intense peaks at (0 0 3), (1 0 1) and (1 0 4) suggest that the $LiNi_{0.5}Mn_{0.5}O_2$ products have the basic Mn(Ni)–O–Mn(Ni) ... units that make up the layered compound [25]. All the peaks are indexable based on the α-$NaFeO_2$-type structure (space group $R\bar{3}m$). The oxygen sub-lattice in the α-$NaFeO_2$-type structure forms an fcc lattice with a distortion in the *c* direction, resulting in a clear splitting of the (0 0 6)/(1 0 2) and (1 0 8)/(1 1 0) peaks. If this distortion (in the *c* direction) is

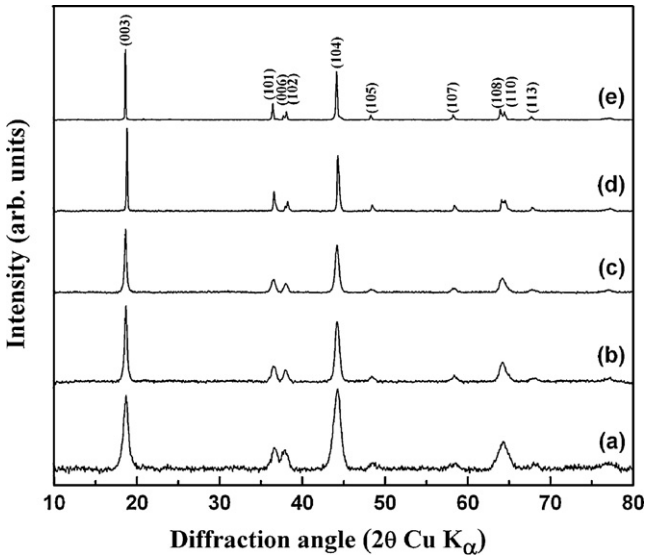

Fig. 1. X-ray diffraction pattern for $LiNi_{0.5}Mn_{0.5}O_2$ cathodes obtained by combustion technique using acenaphthene fuel, calcined at (a) 600 °C, (b) 700 °C, (c) 800 °C, (d) 900 °C and (e) 1000 °C for 12 h.

absent (or if the structure is totally cubic), the (0 0 6)/(1 0 2) and (1 0 8)/(1 1 0) peaks merge into single peaks, as observed with the sample calcined at 600 °C. A good resolution of the (0 0 6)/(1 0 2) and the (1 0 8)/(1 1 0) reflection pairs is typical of an ideal layered structure [26]. Clear separation of the (0 0 6)/(1 0 2) peaks as well as of the (1 0 8)/(1 1 0) peaks can be noticed in the patterns of the materials calcined above 900 °C. The hexagonal doublets such as (0 0 6)/(1 0 2) and (1 0 8/1 1 0) are seen with better splitting than those reported in the literature, which confirms that the synthesized $LiNi_{0.5}Mn_{0.5}O_2$ compound has superior crystallinity, good hexagonal ordering and better layered characteristics [27]. The obtained structure is found to be an ordered layered one, on comparing the Braggs reflections reported in literature [28]. Thus, the newly adopted combustion process with acenaphthene as the fuel is found to be advantageous over the conventional solid state, mixed hydroxide [17] or even the GAC [20] methods traceable in literature. No extraneous peaks, suggesting the presence of impurities, are detected. The crystallite size is obtained using the Scherrer equation for (0 0 3) peak.

The structure parameters of $LiNi_{0.5}Mn_{0.5}O_2$ calcined at different temperatures are provided in Table 1. The intensity ratio of $I_{(003)}/I_{(104)}$ is a sensitive parameter to determine the cation distribution in lattice [29], the higher this ratio the lower is the degree of the cation mixing. Since the value of I_{003}/I_{104} depends on the degree of the displacement between ions located at the 3(a) and 3(b) sites in a space group of $R\bar{3}m$, this value is a measure of the reactivity of lithium insertion materials for a series of $LiNiO_2$ families. According to Makimura and Ohzuku [11], a low value of I_{003}/I_{104} is an indicator of poor electrochemical reactivity due to high concentration of inactive rock-salt domains in a layered solid matrix. The sample calcined at 1000 °C has the highest value for $I_{(003)}/I_{(104)}$ (1.57), while it is the least for the one calcined at 600 °C (0.90). This indicates that the degree of cation mixing decreases with calcination temperature. The degree of cation mixing is much less than that in samples synthesized by a combination of co-precipitation and solid-state reaction as the reported $I_{(003)}/I_{(104)}$ value is only 1.108 [30]. The results are better than those reported in such compounds prepared with GAC method [20] wherein the value is only 0.97. Similar value of less than unity has been obtained by a simple solid state synthesis of layered $LiNi_{0.5}Mn_{0.5}O_2$ directly from a mixture of LiOH, NiO and MnO_2 prepared by ball milling [21]. The values are comparable with the values of about 1.47 reported in samples prepared

Table 1
Structure parameters of $LiNi_{0.5}Mn_{0.5}O_2$ calcined at different temperatures.

Calcined temperature	Crystallite size (nm)	a (Å)	c (Å)	c/a	V (Å)^3	I_{003}/I_{104}	$R = I_{006} + I_{102}/I_{101}$
600 °C	51	2.8876	14.2120	4.9217	102.62	0.9024	–
700 °C	59	2.8959	14.2341	4.9152	103.37	1.2870	–
800 °C	79	2.8944	14.2518	4.9239	103.39	1.3198	–
900 °C	120	2.8955	14.1484	4.8863	102.72	1.5645	0.7353
1000 °C	140	2.8904	14.2905	4.9441	103.39	1.5688	0.7391

with ultrasonic agitation [19]. Also the value is higher than 1.09 reported with glycine assisted sol–gel combustion technique [31]. The $I_{(003)}/I_{(104)}$ values obtained in several investigations inclusive of wet chemical methods have been tabulated and the maximum reported value is about 1.17 [32] and hence the value for compounds prepared by AASC process is the maximum reported value as on date. It is worth mentioning that despite doping the compound with cobalt, the $I_{(003)}/I_{(104)}$ values could not be increased beyond 1.25 [33]. It thus emerges that the use of acenaphthene as a fuel leads to a more crystalline product as compared to common fuels such as sucrose that yield products with $I_{(003)}/I_{(104)}$ values of 1.0–1.2 [34]. It is worth noting that acenaphthene is powerful fuel with a fuel value of 58.

3.2. Surface examinations

3.2.1. Scanning electron microscope

Secondary electron images of the samples (Fig. 2) show that they have a spherical morphology, with particle sizes between 135 and 200 nm for samples calcined at 900 and 1000 °C. The general well-shaped, particle-agglomerated morphology is in agreement with literature reports [35]. The average size of primary particle (about 135 nm) is smaller than about 500 nm reported for this family of compounds prepared by simple solid state methods [7]. The results are in agreement with those of Wu et al. [9] for the material synthesized via an improved solid-state reaction. The larger particle size of the sample calcined at 1000 °C as compared to the 900 °C sample is attributed to sintering. It must be mentioned here that electron microscopy has revealed plate-shaped crystals of 1 μm for $LiNi_{0.5}Mn_{0.5}O_2$ prepared by ion exchange and cubic particles of 0.5 μm for $LiNi_{0.5}Mn_{0.5}O_2$ prepared by a solid state method [3]. It can be seen that individual particles are of submicron size and some of them aggregate to form big particles. Such morphology is quite similar to that of the powder synthesized using the mixed hydroxide method [11,17] and ball mill assisted solid state synthesis [21]. Acenaphthene, as fuel, is better than sucrose [34] in reducing the particle size.

3.2.2. Transmission electron microscope

Transmission electron microscope images of $LiNi_{0.5}Mn_{0.5}O_2$ are shown in Fig. 3. They indicate agglomeration and particle size is about 135 nm, which is in good agreement with the observed XRD pattern. Single particle could be identified. Fig. 3(d) is an electron diffraction (ED) picture of $LiNi_{0.5}Mn_{0.5}O_2$ illustrating its highly crystalline nature.

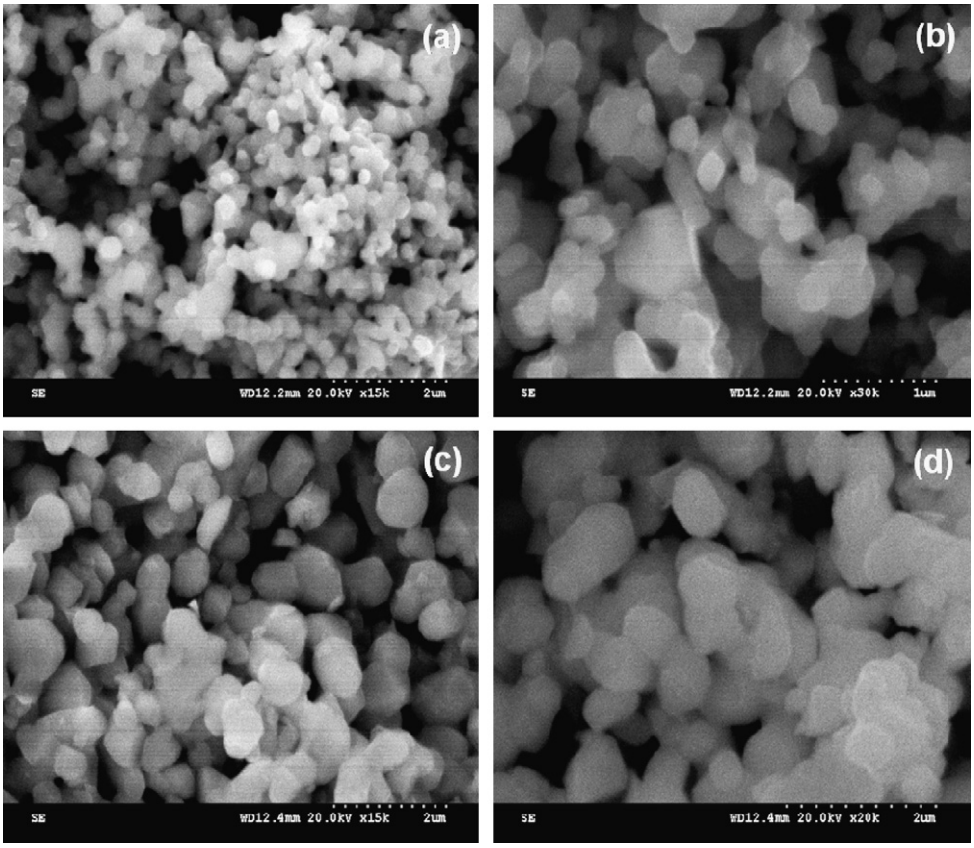

Fig. 2. Scanning electron micrographs for $LiNi_{0.5}Mn_{0.5}O_2$ cathodes obtained by combustion technique using acenaphthene fuel and calcined at 900 °C (a and b) and 1000 °C (c and d).

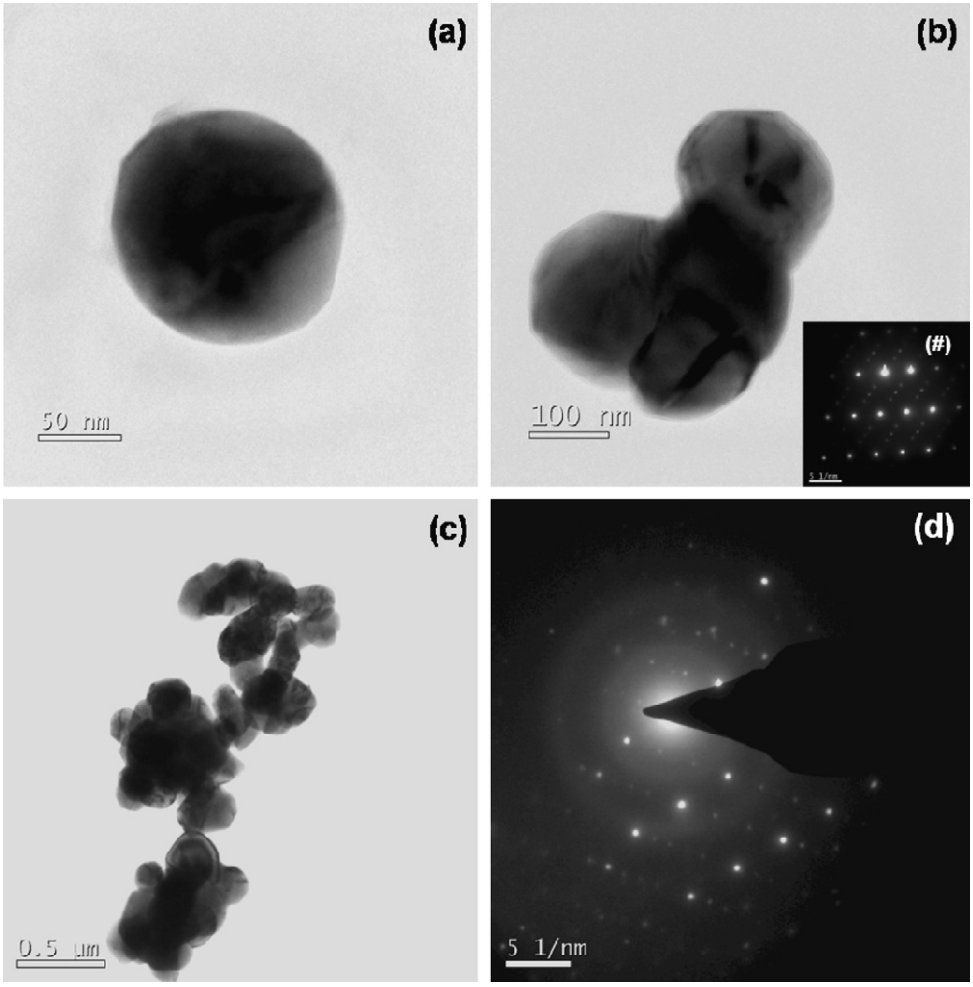

Fig. 3. Transmission electron micrographs and electron diffraction for $LiNi_{0.5}Mn_{0.5}O_2$ cathodes obtained by combustion technique using acenaphthene fuel and calcined at 900 °C.

The particles are more uniform and spherical in nature [36] compared to those synthesized by hydroxide mud method [6]; in addition to reduction in particle size. Even though the particles are slightly bigger than the nano particles (20–30 nm) obtained by Freeze drying synthesis, the particles are comparatively spherical in nature compared to the platelet like nature [37]. In fact the platelet like morphology is much more pronounced in the samples prepared with ultrasonic agitation [19]. Also in contrast to the uniform square morphology obtained by Zhang et al. [19] with ultrasonic agitation, the compound shows uniform spherical morphology. It can be seen that individual particles are of submicron size between 130 and 200 nm and some of them aggregate to form big particles. Such morphology is quite similar to that of the powder synthesized using the mixed hydroxide methods [11,17] and a solid state synthesis [21]. The particles are much finer than that reported with glycine assisted sol–gel combustion method [31]. Also particles synthesized by AASC process are much smaller and more uniform compared to the particle range of 200–350 nm reported by wet-chemical method assisted by tartaric acid [32].

The results show three parallel lines similar to the pattern reported by Arachi et al. [38]. These are indicative of the long range $\sqrt{3}a_{hex} \times \sqrt{3}a_{hex}$ R30° type ordering reflections as reported in literature [35]. However the intensity of the spots depends on the Li intercalation state. Previous electron diffraction studies have revealed long-range cation ordering resulting in a $\sqrt{3}a_{hex} \times \sqrt{3}a_{hex} \times c_{hex}$ supercell with space group $P3_112$ [39,40]. This type of ordering is reported to create two different crystallographic sites, one that is Li-rich and one that is Li-deficient [41] and probably revealed by two different types of superlattice reflections spotted in the picture. But for variations in particle size, the TEM images of agglomerates are similar to the ones reported by Wang et al. [42]. The SEM and TEM images indicate that the particles are well dispersed with average diameter of 135 nm and the size distribution is reasonably good. This is far better than the 1 μm particles obtained by the hydroxide mud method [6]. Also AASC process is better than the wet-chemical method assisted by tartaric acid, wherein the particle size ranged from 200 to 350 nm [32].

3.2.3. X-ray photo electron spectroscopy studies

These studies furnish information on the oxidation states of the metal species present in the synthesized lithiated transition metal oxides. XPS measurements have been done in order to determine the oxidation states of the transition metals in these materials since the oxidation states of manganese and nickel are important for the performance [17,43]. The valence of manganese in $LiNi_{0.5}Mn_{0.5}O_2$ has been determined to be tetravalent by X-ray absorption spectroscopy [44]. The C 1s, Li 1s, Ni 2p, Mn 2p and O 1s XPS core level spectra for the prepared $LiNi_{0.5}Mn_{0.5}O_2$ samples are shown in Fig. 4. The C 1s emission peak is observed around 284.98 eV, which is used as the reference in the present XPS measurements. The binding energy of the Li 1s emission peak is positioned at 50.26 eV and appears as a broad signal. The Ni 2p XPS spectrum in Fig. 4(c) consists of the characteristic broad satellite peak with the BE at

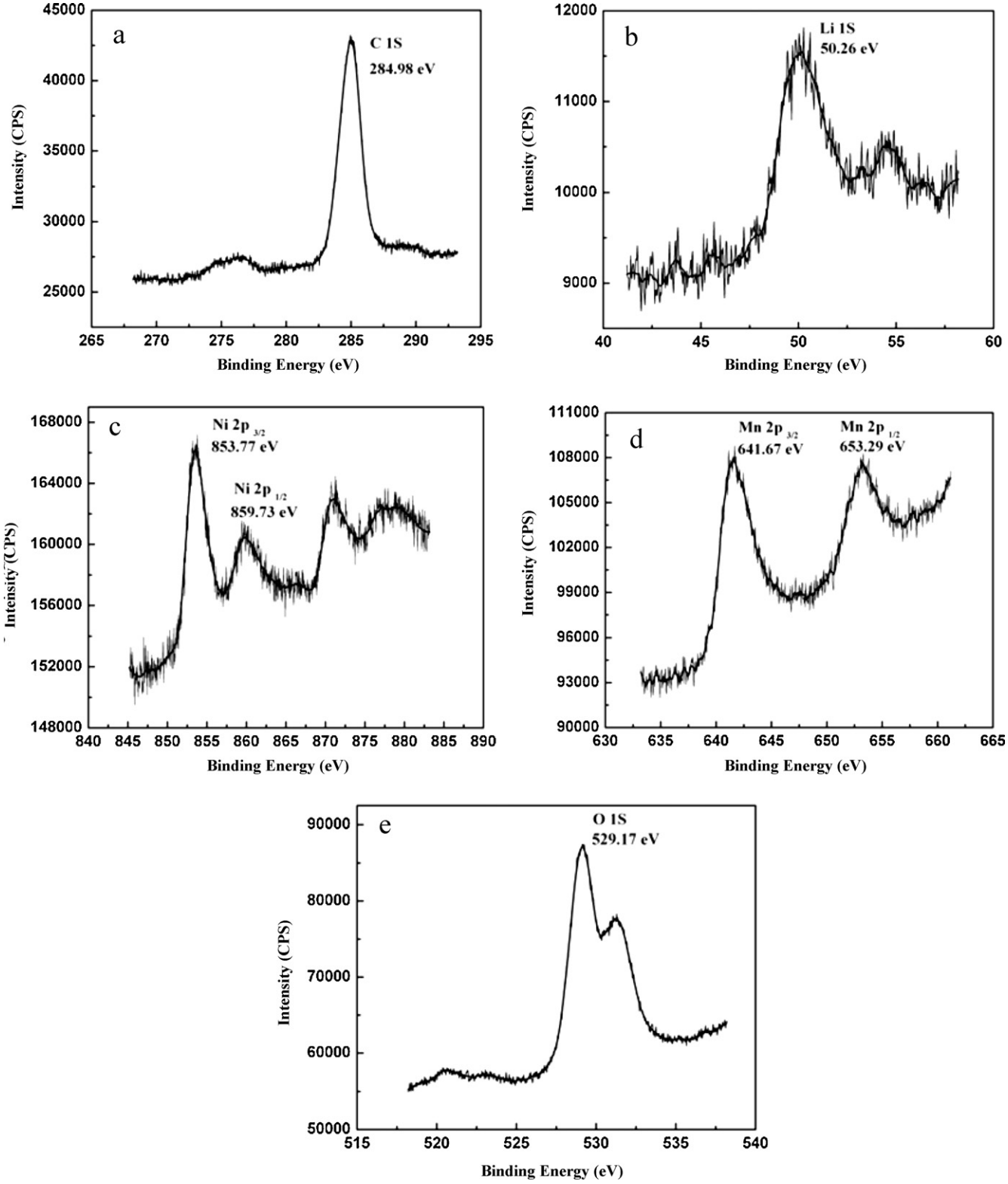

Fig. 4. X-ray photoelectron spectroscopy of $LiNi_{0.5}Mn_{0.5}O_2$ materials (a) C 1s, (b) Li 1s, (c) Ni 2p, (d) Mn 2p, and (e) O 1s.

859.73 eV. Such broad satellite peaks are present in Ni-containing oxides, such as NiO, $LiNiO_2$, $LiNi_{1/3}Co_{1/3}Mn_{1/3}O_2$ and in the spinel, $LiMn_{1.5}Ni_{0.5}O_4$ [45,46]. The satellite peak is explained due to the multiple splitting in the energy levels of the Ni-oxides [46,47]. The BE of the center of Ni $2p_{3/2}$ peaks of $LiNi_{0.5}Mn_{0.5}O_2$ has been reported as 854.2 eV [30]. The observed higher BE value observed in compounds prepared by AASC process can be attributed to the presence of nickel in both 2+ and 3+ oxidation states. The BE value of Mn $2p_{3/2}$ peak at 642.4 eV is typical for Mn^{4+} oxidation state [48], however, the presence of Mn^{3+} with Mn^{4+} will result in the Mn $2p_{3/2}$ peak shifting to a lower BE. O 1s spectra show an interesting progression with the preparation method. The BE value of the O 1s component is located at 529.17 eV, originating from Ni–O and Mn–O in the synthesized material. The analysis of contents of

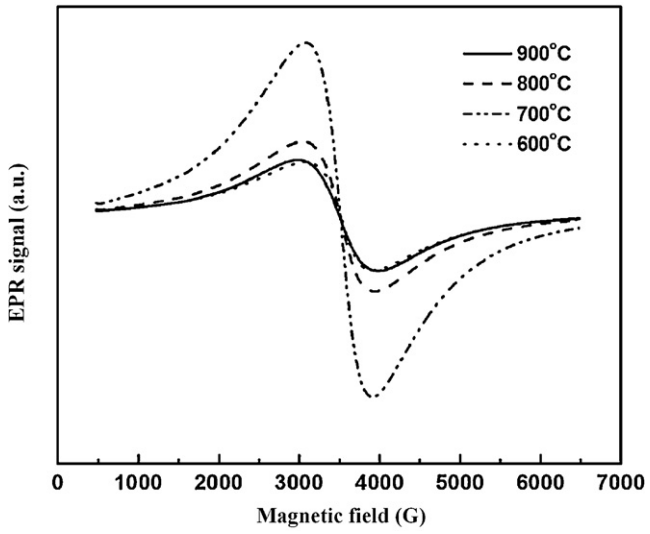

Fig. 5. EPR spectra for $LiNi_{0.5}Mn_{0.5}O_2$ cathodes obtained by combustion technique using acenaphthene fuel, calcined at different temperature for 12 h.

metal ions from XPS also suggests that the molar ratios of the metal elements in the prepared samples are in good agreement with their stoichiometric proportion.

3.3. Spin resonance investigations

3.3.1. Electron paramagnetic resonance studies

The electrochemical performance of these electrode materials is strongly dependent on synthesis procedures [15] as they yield products with different cation distributions [49]. Cation distribution in the transition metal layers can be investigated by EPR spectroscopy, which has been used to obtain information $LiNi_{0.5}Mn_{0.5}O_2$ prepared under atmospheric [14] and high pressure conditions [28]. Changes in the manganese environment during lithium extraction/insertion can also be monitored by EPR spectroscopy.

$LiNi_{0.5}Mn_{0.5}O_2$ contains two magnetic ions, Ni^{2+} and Mn^{4+}. Ni^{2+} is a non-Kramers ion since it has even number of d-electrons and its EPR spectra is sensitive to the environment. As a consequence, the EPR signal of Ni^{2+} can then be detected only when the ion is present as a residual impurity [50]. If the concentration of the ion is large, as in the present case, the distribution of crystal fields and strains on the different sites smear out the resonance spectra and can no longer be detected. This is the reason why Ni^{2+} does not contribute to the EPR spectrum. The detected paramagnetic resonance could only be attributed to the presence of Mn^{4+} ions that carry a half-integer spin ($S = 3/2$) and are then EPR-active.

The EPR spectra are shown in Fig. 5. The EPR spectrum of pristine sample consists of one signal with a Lorentzian line shape and is indicative of the ordered nature of the sample [28].

The position of the center of the signal is close to 3450 G. This is somewhat deviated from the position expected for uncorrelated spins with the gyromagnetic factor $g = 2.033$ [32]. The line width ΔB is small, namely 900 G at room temperature. Earlier studies have reported the value around 1280 G [32]. The signal intensity, however, diminishes on lowering the temperature. Since Ni^{3+} is in the low-spin state [38], the contribution from Ni^{3+} is only minimal. Also absence of smearing of EPR resonance reveals absence of Ni^{3+}.

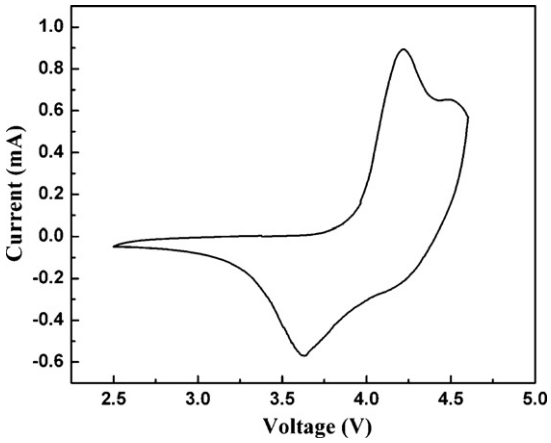

Fig. 6. Cyclic voltammograms of the synthesized $LiNi_{0.5}Mn_{0.5}O_2$ obtained in the voltage range 2.5–4.6 V at scanning rate 0.1 mV s^{-1}.

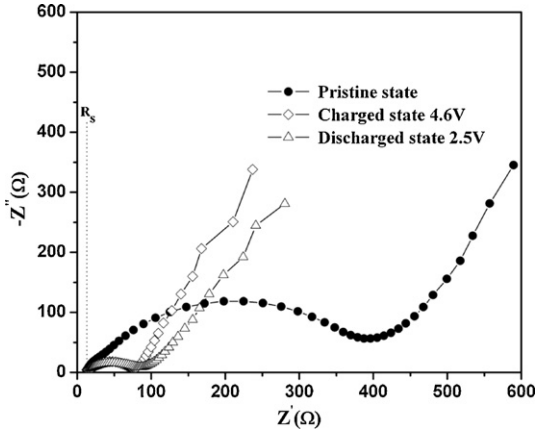

Fig. 7. EIS complex impedance plots of the half cell with the 900 °C calcined $LiNi_{0.5}Mn_{0.5}O_2$ as cathode, at the state of pristine, charged (4.6 V) and discharged (2.5).

3.4. Electrochemical performance

3.4.1. Cyclic voltammetry

Cyclic voltammograms of cells of configuration Li/electrolyte/$LiNi_{0.5}Mn_{0.5}O_2$ and cycled between 2.5 and 4.6 V at the scan rate of 0.1 mV s^{-1} have been investigated. Typical cyclic voltammograms are shown in Fig. 6. The transition-metal layer in $LiNi_{0.5}Mn_{0.5}O_2$ is bi-functional, with Ni^{2+} acting as a double redox-active center [13,51,52] and Mn^{4+} providing stability to the host structure [53]. The absence of any peak around 3 V suggests that no Mn^{3+} is present [54] in the samples. An anodic peak at 4.0–4.2 V and a corresponding cathodic peak at 3.6 V can be noted. These redox peaks are also signatures of hexagonal phase in these types of layered compounds and indicate perfect reversibility. The peaks could be assigned to the Ni^{4+}/Ni^{2+} couple. Furthermore, a very low intensity high voltage broad hump can also be discerned from the oxidation process at around 4.41 V, which can be attributed to Mn^{4+} ions in the samples. The absence of a true peak at 4.41 V in the de-intercalation process suggests the electrochemical inactivity of manganese in this compound. The faintly detectable high voltage hump exhibited by pristine $LiNi_{0.5}Mn_{0.5}O_2$ is similar to observations noted earlier [31,55], and could probably be ascribed to small particle sizes of the samples. The cathodic peak around 3.6 V corresponds to the voltage plateau of the discharge processes of the cell used. The broad anodic and cathodic peaks observed with this material contrast with the sharp

peaks observed with $LiNiO_2$, which shows three distinct phase transitions [56]. The absence of such multi-phase reactions can mean a lower level of structural degradation upon cycling in the case of $LiNi_{0.5}Mn_{0.5}O_2$. The difference between anodic potential φ_{pa} and cathodic potential φ_{pc}, $\Delta\varphi_p = \varphi_{pa} - \varphi_{pc}$, is a measure of the reversibility of the intercalation process: the lower the value of $\Delta\varphi_p$, the better reversibility. The potential difference $\Delta\varphi_p$ is about 0.6 V, which is higher than the 0.36 V reported by Zhang et al. [30] and 0.19 V reported for $LiNi_{0.4}Mn_{0.4}Co_{0.2}O_2$ prepared by a self-combustion reaction with sucrose as a fuel [34]. Also the oxidation peak is shifted to the right 0.1 V whereas the reduction peak is shifted to the left by 0.25 V. Since only one cathodic peak is seen in contrast to the additional secondary peaks observed by Zhang et al. [30], it implies that the phase purity of the compounds prepared with acenaphthene as a fuel is higher, which corroborates with XRD patterns that show no extraneous peaks. It must be noted that some samples have been shown to exhibit three couples of sharp redox peaks due to the insert of different phases [44] in such class of materials. However, the absence of such multiple redox peak couples in the compounds synthesized by AASC process is a further evidence of phase purity. The oxidation state of manganese in $LiNi_{0.5}Mn_{0.5}O_2$ is invariant at 4+, as evidenced by the absence of the redox reaction around 3.0 V corresponding to the Mn^{4+}/Mn^{3+} couple [54,57]. The cyclic voltammograms are reversible over several cycles, suggesting good reversibility for the electrode processes. The results are somewhat similar to those prepared by ball mill assisted solid state synthesis of layered $LiNi_{0.5}Mn_{0.5}O_2$ directly from a mixture of LiOH, NiO and MnO_2, i.e., 4–3.6 V [21], but the electrochemical performance is far more superior.

3.4.2. Electrochemical impedance spectroscopy

This is a powerful technique to study the kinetics of lithium intercalation/deintercalation processes [58,59]. EIS has been carried out in the pristine state, fully charged state (charged to 4.6 V at 0.1 C rate), and in the fully discharged state (discharged to 2.5 V at 0.1 C rate). EIS data has been collected after ageing the fabricated lithium ion cell for 24 h. Nyquist plots of the charged and discharged electrodes were recorded after allowing 1 h of stabilization period. Nyquist plots of pristine state, charged state and discharged state of the Li-ion cell are shown in Fig. 7. The pristine sample shows a high-frequency semicircle and a sloping line in the low-frequency region. The resistance component, R_s, arises from the electrolyte and other cell constituents. The semicircle is attributed to the lithium ion migration through the interface between the surface layer of the particles and the electrolyte, as suggested by Aurbach et al. [60,61]. The semicircle in the case of the charged electrode is attributed to the formation of a solid electrolyte interphase (SEI). A lower resistance of 325 Ω, however, is observed in the charged state and can be related to destruction or modification of the inactive SEI due to current flux [62,63]. The Nyquist plots of the charged and discharged electrodes are not very different, except that there is a marginal in resistance in the discharged state, which agrees with earlier results [63,64].

3.4.3. Charge–discharge studies

The voltage-capacity profiles of $LiNi_{0.5}Mn_{0.5}O_2$ cathodes obtained by AASC process at 0.1 C rate are shown in Fig. 8. There is only one voltage plateau on both charge and discharge curves. This is consistent with the results in cyclic voltammetry experiments, which display current peaks corresponding to only one redox couple. The results are better than the performance of the compound prepared by an improved solid state reaction of Wu et al. [9] as the voltage range is high. Moreover, the irreversible capacity in the first cycle is negligible as compared to that reported for $LiNi_{0.5}Ti_{0.5}O_2$ [65]. Additionally, the capacity decay upon cycling is small (on an average 1.16 mAh g^{-1} per cycle during the first five cycles), which progressively reduces with cycling (on an average 0.90 mAh g^{-1} per cycle between cycle numbers 46 and 50). The differences between the charging and discharging voltages also decrease upon cycling. The low over-voltage is a welcome feature of this material. It is worth noting that the coulombic efficiency rises from 96.58% at first cycle to 99.56% at fiftieth cycle. The marginal voltage drop observed during the first charging process could be ascribed to the reaction of the traces of metallic nickel contained in the sample [65].

The galvanostatic cycling behavior of $LiNi_{0.5}Mn_{0.5}O_2$ calcined at 900 and 1000 °C for 12 h is depicted in Fig. 9. Coin cell delivered an initial discharge capacity of 161 mAh g^{-1} for the cathodes heated at 900 °C. This is as per expectations based on structural properties. The capacity fading in such material is related to an increase in the ohmic drop in case of prolonged cycling. One mechanism of capacity fading is the dissolution of active material in the electrolyte during cycling. This dissolution is generally attributed to the existence of HF, which is easily formed when using $LiPF_6$ as the electrolyte salt. The discharge results are similar to the reported capacity decrease of such materials subjected to high-temperature

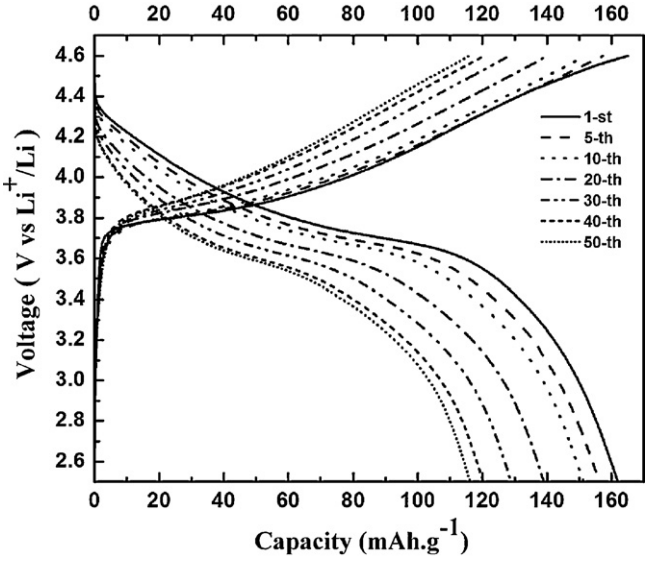

Fig. 8. Galvanostatically voltage vs capacity profile of calcined at 900 °C for a cell $Li/LiNi_{0.5}Mn_{0.5}O_2$ in the voltage range from 2.5 to 4.6 at 0.1 C rate.

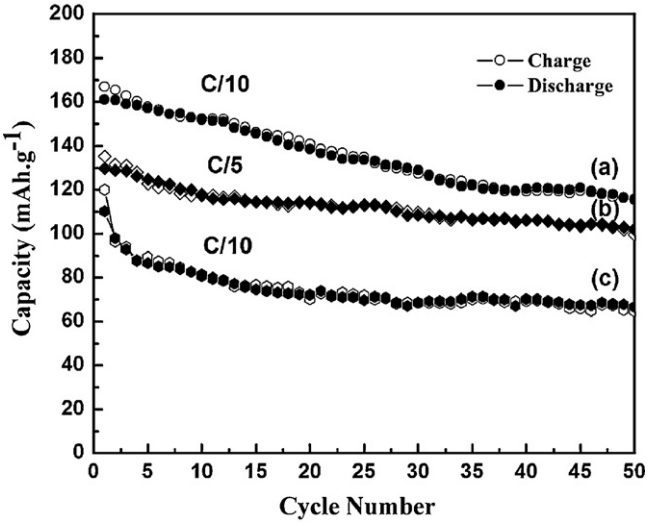

Fig. 9. Capacity vs cycle number plot for synthesized $LiNi_{0.5}Mn_{0.5}O_2$ materials calcined at 900 °C (a), (b) and 1000 °C and (c) for 12 h.

processing [66]. An increase in the processing temperature to 1000 °C leads to a reduction in capacity, an observation similar to that of Shlyakhtin et al. [67]. This reduction is ascribed to faster annealing of defects and partial conversion into structurally stable, but less active, secondary phases such as $LiMn_2O_4$, Li_2MnO_3, etc. [67], which seems to contravene a marginal increase in the $I_{(003)}/I_{(104)}$ values. Also, a reasonable performance with reduced capacity fading is obtained even at higher discharge rates (Fig. 9(b)).

The observed superior performance could be attributed to the lesser degree of cation mixing since coulombic efficiencies and discharge performance are related to cation mixing in the host structure. Ni^{2+} ions located at the octahedral Li sites can block Li^+ intercalation and diffusion. Consequently, a gradual capacity fading for $LiNi_{0.5}Mn_{0.5}O_2$ [43] arises as seen from cycle life curves. It is, however, possible to modify the heating protocol to improve the electrochemical properties of layered $LiNi_{0.5}Mn_{0.5}O_2$ [9], including its cycle life. The performance of $LiNi_{0.5}Mn_{0.5}O_2$ prepared by AASC process is comparable to those prepared by hydroxyl mud [6], mixed hydroxide [13] and freeze drying methods [37] as well as those with layered single-crystalline $LiNi_{0.5}Mn_{0.5}O_2$ nanostructures [42] synthesized through a citric acid-assisted sol–gel method. The products in this study, however, outperform that obtained by a glycine-assisted combustion synthesis [31], wet-chemical method assisted by tartaric acid [32] and ball mill assisted solid state synthesis [21]. The cycle life experiments indicate a higher capacity than the materials prepared by co-precipitation and in the particle range 3–10 μm [68].

4. Conclusions

Pristine $LiNi_{0.5}Mn_{0.5}O_2$ materials are prepared by a novel AASC process for the first time. The structure and electrochemical properties are systematically studied and compared with the properties of $LiNi_{0.5}Mn_{0.5}O_2$ prepared by other methods. The sample has a lesser degree of cation mixing as compared to the similar samples prepared by other methods. The particle sizes of the products are also much smaller and approaching the nano range compared to the other synthesis routes. The optimum synthesis temperature and time are 900 °C and 12 h, respectively. The initial discharge capacity of layered $LiNi_{0.5}Mn_{0.5}O_2$ prepared under above conditions is 161 mAh g^{-1} and the sample displays an excellent lithium intercalation/deintercalation.

Acknowledgements

The authors are thankful to the Council of Scientific and Industrial Research (CSIR), India for financial support through IAP-04 to carry out this work.

References

[1] J.M. Tarascon, D. Guyomard, G.L. Baker, J. Power Sources 44 (1993) 689–700.
[2] J. Breger, N. Dupré, P.J. Chupas, P.L. Lee, T. Proffen, J.B. Parise, C.P. Grey, J. Am. Chem. Soc. 127 (2005) 7529–7537.
[3] K. Kang, Y.S. Meng, J. Bréger, C.P. Grey, G. Ceder, Science 311 (2006) 977–980.
[4] F. Mizuno, A. Hayashi, K. Tadanaga, T. Minami, M. Tatsumisago, J. Power Sources 124 (2003) 170–173.
[5] B.L. Cushing, J.B. Goodenough, Solid State Sci. 4 (2002) 1487–1493.
[6] S.H. Na, H.S. Kim, S.I. Moon, Electrochim. Acta 50 (2004) 449–452.
[7] D.C. Li, T. Muta, H. Noguchi, J. Power Sources 135 (2004) 262–266.
[8] T. Ohzuku, Y. Makimura, Chem. Lett. 30 (2001) 744–745.
[9] Q. Wu, X. Li, M. Yan, Z. Jiang, Electrochem. Commun. 5 (2003) 878–882.
[10] K. Ariyoshi, S. Yamamoto, T. Ohzuku, J. Power Sources 119–121 (2003) 959–963.
[11] Y. Makimura, T. Ohzuku, J. Power Sources 119–121 (2003) 156–160.
[12] C.S. Johnson, J.S. Kim, A.J. Kropf, A.J. Kahaian, J.T. Vaughey, L.M. Fransson, K. Edstrom, M.M. Thackeray, Chem. Mater. 15 (2003) 2313–2322.
[13] Z. Lu, D.D. MacNeil, J.R. Dahn, Electrochem. Solid State Lett. 4 (2001) A191–A194.
[14] R. Stoyanova, E. Zhecheva, S. Vassilev, J. Solid State Chem. 179 (2006) 378–388.
[15] D.A.R. Barkhouse, J.R. Dahn, J. Electrochem. Soc. 152 (2005) A746–A751.
[16] Y. Hinuma, Y.S. Meng, K. Kang, G. Ceder, Chem. Mater. 19 (2007) 1790–1800.
[17] Z. Lu, L.Y. Beaulieu, R.A. Donaberger, C.L. Thomas, J.R. Dahn, J. Electrochem. Soc. 149 (2002) A778–A791.
[18] J. Cho, Y. Kim, G. Kim, J. Phys. Chem. C 111 (2007) 3192–3196.
[19] B. Zhang, G. Chen, P. Xu, Z. Lv, Solid State Ionics 178 (2007) 1230–1234.
[20] P. Periasamy, N. Kalaiselvi, J. Power Sources 159 (2006) 1360–1364.
[21] H. Xia, S.B. Tang, L. Lu, J. Alloys Compd. 449 (2008) 296–299.
[22] H.-Q. Lu, F. Wu, Y.-F. Su, N. Li, S. Chen, L.Y. Bao, Wuli Huaxue Xuebao Acta Phys. Chim. Sin. 26 (2010) 51–56.
[23] Y.J. Park, Y.S. Hong, X. Wu, M.G. Kim, K.S. Ryu, S.H. Chang, J. Electrochem. Soc. 151 (2004) A720–A727.
[24] K.C. Patil, Bull. Mater. Sci. 16 (1993) 533–541.
[25] S. Lai, C. Hu, Y. Li, D. Luo, M. Cao, Z. Yu, H. Liu, Solid State Ionics 179 (2008) 1754–1757.
[26] R.J. Gummow, M.M. Thackeray, W.I.F. David, S. Hull, Mater. Res. Bull. 27 (1992) 327–337.
[27] G.T.K. Fey, Z.F. Wang, T.P. Kumar, Ionics 8 (2002) 351–359.
[28] M. Yoncheva, R. Stoyanova, E. Zhecheva, R. Alcántara, G. Ortiz, J.L. Tirado, J. Solid State Chem. 180 (2007) 1816–1825.
[29] T. Ohzuku, A. Ueda, M. Nagayama, J. Electrochem. Soc. 140 (1993) 1862–1870.
[30] B. Zhang, G. Chen, P. Xu, C.C. Li, J. Power Sources 176 (2008) 325–331.
[31] S. Gopukumar, K.Y. Chung, K.B. Kim, Electrochim. Acta 49 (2004) 803–810.
[32] A. Abdel-Ghany, K. Zaghib, F. Gendron, A. Mauger, C.M. Julien, Electrochim. Acta 52 (2007) 4092–4100.
[33] D.C Li, H. Noguchi, M. Yoshio, Electrochim. Acta 50 (2004) 427–430.
[34] S.K. Martha, H. Sclar, Z.S. Framowitz, D. Kovacheva, N. Saliyski, Y. Gofer, P. Sharon, E. Golik, B. Markovsky, D. Aurbach, J. Power Sources 189 (2009) 248–255.
[35] D. Mohanty, P. Paudel, H. Gabrisch, Solid State Ionics 181 (2010) 914–920.
[36] S.H. Ju, Y.C. Kang, J. Alloys Compd. 469 (2009) 304–309.
[37] O.A. Shlyakhtin, Y.S. Yoon, S.H. Choi, Y.J. Oh, Electrochim. Acta 50 (2004) 505–509.
[38] Y. Arachi, H. Kobayashi, S. Emura, Y. Nakata, M. Tanaka, T. Asai, H. Sakaebe, K. Tatsumi, H. Kageyama, Solid State Ionics 176 (2005) 895–903.
[39] Y.S. Meng, G. Ceder, C.P. Grey, W.S. Yoon, M. Jiang, J. Breger, Y. Shao-Horn, Chem. Mater. 17 (2005) 2386–2394.
[40] Y.S. Meng, G. Ceder, C.P. Grey, W.S. Yoon, Y. Shao-Horn, Electrochem. Solid State Lett. 7 (2004) A155–A158.
[41] H.H. Li, N. Yabuuchi, Y.S. Meng, S. Kumar, J. Breger, C.P. Grey, Y. Shao-Horn, Chem. Mater. 19 (2007) 2551–2565.
[42] X. Wang, F. Zhou, X. Zhao, Z. Zhang, M. Ji, C. Tang, T. Shen, H. Zheng, J. Cryst. Growth 267 (2004) 184–187.
[43] S.T. Myung, S. Komaba, N. Hirosaki, K. Hosoya, N. Kumagai, J. Power Sources 146 (2005) 645–649.
[44] W.S. Yoon, Y. Paik, X.-Q. Yang, M. Balasubramanian, J. McBreen, C.P. Grey, Electrochem. Solid State Lett. 5 (2002) A263–A266.
[45] K.M. Shaju, G.V. Subba Rao, B.V.R. Chowdari, Electrochim. Acta 48 (2002) 145–151.
[46] A.F. Carley, S.D. Jackson, J.N. O'Shea, M.W. Roberts, Surf. Sci. 440 (1999) L868–L874.
[47] K. Amine, H. Tukamoto, H. Yasuda, Y. Fujita, J. Electrochem. Soc. 143 (1996) 1607–1613.
[48] K.M. Shaju, G.V. Subba Rao, B.V.R. Chowdari, Electrochim. Acta 48 (2003) 1505–1514.
[49] E. Zhecheva, R. Stoyanova, R. Alcaïntara, P. Lavela, J.L. Tirado, Pure Appl. Chem. 74 (2000) 1885–1894.
[50] P.J. Alonso, R. Alcala, J.M. Spaeth, Phys. Rev. B 41 (1990) 10902–10905.
[51] J. Reed, G. Ceder, Electrochem. Solid State Lett. 5 (2002) A145–A148.
[52] J.M. Paulsen, J.R. Dahn, J. Electrochem. Soc. 147 (2000) 2478–2485.
[53] M.M. Thackeray, Solid State Chem. 25 (1997) 1–71.
[54] J.M. Paulsen, C.L. Thomas, J.R. Dahn, J. Electrochem. Solid State Lett. 147 (2000) 861–869.
[55] S.H. Kang, J. Kim, M.E. Stoll, D. Abraham, Y.K. Sun, K. Amine, J. Power Sources 112 (2002) 41–48.
[56] W. Li, J.N. Reimers, J.R. Dahn, Solid State Ionics 67 (1993) 123–130.
[57] K.M. Shaju, G.V.S. Rao, B.V.A. Chowdari, Electrochem. Commun. 4 (2002) 633–638.
[58] M.D. Levi, K. Gamolsky, D. Aurbach, U. Heider, R. Oesten, Electrochim. Acta 45 (2000) 1781–1789.
[59] K.M. Shaju, G.V. Subba Rao, B.V.R. Chowdari, J. Electrochem. Soc. 150 (2003) A1–A13.
[60] D. Aurbach, M.D. Levi, E. Levi, H. Teller, B. Markovsky, G. Salitra, J. Electrochem. Soc. 145 (1998) 3024–3034.
[61] M.D. Levi, G. Salitra, B. Markovsky, H. Teller, D. Aurbach, U. Heider, L. Heider, Electrochem. Soc. 146 (1999) 1279–1289.
[62] B. Markovsky, D. Kovacheva, Y. Talyosef, M. Gorova, J. Grinblat, D. Aurbach, Electrochem. Solid State Lett. 9 (2006) A449–A453.
[63] K.M. Shaju, G.V.S. Rao, B.V.R. Chowdari, Electrochim. Acta 49 (2004) 1565–1576.
[64] G. Ning, B. Haran, B.N. Popov, J. Power Sources 117 (2003) 160–169.
[65] M. Tsuda, H. Arai, M. Takahashi, H. Ohtsuka, Y. Sakurai, K. Sumitomo, H. Kageshima, J. Power Sources 144 (2005) 183–190.
[66] J.H. Kim, C.S. Yoon, Y.K. Sun, J. Electrochem. Soc. 150 (2003) A538–A542.
[67] O.A. Shlyakhtin, S.H. Choi, Y.S. Yoon, Y.J. Oh, J. Power Sources 141 (2005) 122–128.
[68] K.S. Lee, S.T. Myung, J.S. Moon, Y.K. Sun, Electrochim. Acta 53 (2008) 6033–6037.